Tertiary Structure of Ganglioside G_A1

Bull. Korean Chem. Soc. **1998**, Vol. 19, No. 5   569

Tertiary Structure of Ganglioside G_{A1}
Determined by NMR Spectroscopy

Kyungik Lee, Sangwon Lee, Gil-Ja Jhon[†], and Yangmee Kim[*]

Department of Chemistry, Konkuk University, Seoul 143-701, Korea
†Department of Chemistry, Ewha Womans University, Seoul 120-750, Korea
Received February 2, 1998

Investigation of the structure of the gangliosides has proven to be very important in the understanding of their biological roles. We have determined the tertiary structure of asialoganglioside G_{M1} (G_{A1}) using NMR spectroscopy and distance geometry calculations. All of the structures are very similar except the glycosidic torsion angles in the ring IV and ring III linkages. There are two low-energy structures for GA1, G1 and G2. G1 differs from G2 only in the IV-III glycosidic linkages and the orientation of acetamido group in ring III. There is a stable intramolecular hydrogen bond between the third hydroxyl group in ring I and the ring oxygen atom in ring II. Also, there may be a weak hydrogen bond between the second hydroxyl group in ring IV and the acetamido group in ring III. Small coupling constants of $^3J_{IIH3,IOH3}$ and $^3J_{IVH2,IVOH2}$ support this result. Overall structural features of G_{A1} are very similar to those of G_{M1}. It implicates that specificities of the sugar moieties in G_{M1} are caused not by their tertiary foldings, but mainly by the electrostatic interactions between the polar sialic acid and its receptors. Since it is evident that G_{A1} is more hydrophobic than G_{M1}, a receptor with a hydrophobic binding site can recognize the G_{A1} better than G_{M1}. Studies on the conformational properties of G_{A1} may lead to a better understanding of the molecular basis of its functions.

Introduction

Carbohydrates have long been thought of as recognition elements because of their unique ability to generate a vast repertoire of structures using only simple sugars made even more diverse by the variety of sugar-sugar linkages that can occur.[1] Cell-surface oligosaccharides, such as those which occur in the head groups of glycolipids, display a diversity in both primary structure and tertiary conformation that makes them useful mediators of cell-specific interactions. Gangliosides are sialic acid-containing glycosphingolipids found in the plasma membrane of animal cells, being particularly abundant in the nervous system.[2,3] They are asymmetrically located in the outer face of the membrane with the complex carbohydrate head groups, which extend beyond the surface of the cell, interacting with a variety of external ligands. Gangliosides may be included in the process of specific recognition of signal molecules at the membrane surface and signal transduction through the membrane.[4,5] There are considerable evidences that gangliosides have various functions in many processes including cell growth, development, differentiation, antigenicity, and receptor action. Recently, G_{M1} has been found to alleviate genetic and lesion-induced memory deficits.[6] The oligosaccharide moieties function as structure-specific epitopes in biological recognition.[7] Therefore, there is a growing need to determine the three-dimensional structure of gangliosides.

The cell adhesion field provides an important opportunity in which to explore the function of oligosaccharides at the cell surface. Asialoganglioside G_{M1} (G_{A1}; β-D-Gal-(1→3)-β-D-GalNAc-(1→4)-β-D-Gal-(1→4)-β-D-Glc-1-O-Cer) is found as a receptor of *Bordetella pertussis*, which is a common human respiratory pathogen.[8] *Pseudomonas aeru-ginosa*, which is a gram-negative opportunistic bacterial pathogen, and *Candida albicans*, which is an opportunistic fungal pathogen, have been shown to bind to G_{A1} receptor.[9,10] *C. albicans*-mediated adherence to buccal epithelial cells utilizes both G_{A1} and asialo G_{M2} receptors.[11] Adherence of bacteria to specific cellular receptors is the initial event in many infectious diseases.

The identification of the sugar moiety of G_{A1} as the receptor for *Pseudomonas* raises the possibility that ligands to this sugar or other compounds resembling the receptor in a three-dimensional structure might prevent the initial colonization with *P. aeruginosa* and *S. aureus* and serve as another type of antibacterial therapy. An understanding of the three-dimensional structure of the G_{A1} head group may provide valuable insights into research in antibacterial therapy.

The three-dimensional (3D) structures of biopolymers are known to play an important roles in a variety of biological functions. In many cases, the crystal structures of carbohydrates are not available. At present the best method with which to study solution structure of gangliosides with accuracy is high-resolution NMR spectroscopy. Recently, conformations of some gangliosides have been determined by NMR spectroscopy and molecular modeling.[12–16] In order to determine the three-dimensional structure of a ganglioside by NMR spectroscopy, the assignment of the spectrum and measurement of NOEs are prerequisites. We have previously reported the assignment of ^1H and ^{13}C resonances of G_{A1}.[17] NMR experiments on gangliosides provide a very limited number of NOE distance constraints, and this is a problem common to all oligosaccharides.[18–20] In this study we performed NMR experiments on G_{A1} in 98:2 DMSO-d_6-D$_2$O and in 100% DMSO-d_6 to extract NOEs from all protons as many as possible, including both of nonexchangeable and exchangeable protons. Unexchanged hydroxyl protons can provide important information about

the hydrogen bonds as they exist in G_{A1}.[21] We utilized distance geometry calculation for the first time to generate the tertiary structure of ganglioside. Here, we report the tertiary structure of G_{A1} as determined by NMR spectroscopy and distance geometry calculations. Based on this structure, the antigenic function of G_{A1} will be discussed.

Experimental

NMR spectroscopy. G_{A1} was purchased from Sigma Chemical Co. For the assignment and NOE integration of nonexchangeable protons, G_{A1} was deuterium-exchanged by repeated lyophilization from DMSO-d_6-D_2O mixture and finally dissolved in 0.4 mL of 98:2 DMSO-d_6-D_2O solvent for NMR spectroscopy that made a 7 mM sample. For the spectral assignments and NOE integrations of all the protons, including exchangeable protons, G_{A1} was dissolved in 100% DMSO-d_6. Chemical shifts of ^1H and ^{13}C resonances are expressed relative to an internal TMS signal at 0 ppm.

All the phase-sensitive two-dimensional experiments such as TOCSY,[22] NOESY,[23] DQF-COSY,[24] and ROESY[25] experiments were performed using the TPPI method. For these experiments, 512 transients with 2 K complex data points were collected for each of the increments with a relaxation delay of 1.2-2.0s between successive transients. Data were recorded with 64 scans for each of the t_1 increments with a spectral width of 4504.5 Hz in both dimensions. For the measurement of coupling constants, the DQF-COSY spectrum was acquired with 4 K complex data points and processed with 4 K × 2 K matrix, giving a resolution of 1.0 Hz/point. A high-resolution 1D spectrum (64 K) was acquired as well to determine the coupling constant accurately. For the NOE integrations, NOESY and ROESY experiments were conducted using mixing times of 150, 200, and 250 ms at 298 K, 303 K, and 313 K. Prior to Fourier transformation, either a shifted skewed sinebell weighting function or a Gaussian function were applied to give a final data matrix of 1024 × 1024 real points of NOESY spectra. In order to calculate temperature coefficients, chemical shifts were measured from 298 K to 333 K at every 5°. All spectra were recorded on a 500-MHz spectrometer in the Inter-University Center for Natural Science Research Facilities in Seoul National University and the Korea Basic Research Science Institute. All NMR spectra were processed offline using the FELIX software package[26] on SGI workstation in our laboratory.

Calculation of tertiary structure of G_{A1}. Distance geometry calculations were performed using DGII program.[26,27] For the calibration of distance constraints, H1-H5 distances in β-D-Glc and β-D-Gal are set to 2.4 Å, and H1-H2 in β-D-Glc and H2-H3 in β-D-Gal are set to 3.1 Å. These distances are the values provided in the AMBER-minimized structures. Interproton distance restraints were derived from NOEs assigned in the 2D NOESY spectra acquired with a mixing time of 150 ms. The NOE-derived distances were divided into three classes: 1.8-2.5 Å for the strong peaks, 2.5-3.5 Å for the medium peaks, and 3.5-5.0 Å for the weak peaks. For the strong peaks, the upper bounds were corrected by adding 0.2 Å to the measured distances. For the medium peaks, they were corrected by adding 0.3 Å. For the weak peaks, they are corrected by adding 0.5 Å.

The lower bounds were fixed to the van der Waals radius. Pseudoatom correction was made by adding additional 1.0 Å to the upper bounds for methyl protons in acetamido group of ring III.

As shown in Table 2, the restraint file is consisted of 17 interresidual NOEs, 4 NOEs between the amido proton in β-D-GlcNAc and the protons in the same ring III, and also intraresidual NOEs (not listed here). For the structural calculation, we used AMBER force field. In this forcefield, Homans forcefield for oligosaccharides is incorporated.[28] It also accounts the anomeric effect associated with carbohydrates. It is available in the DISCOVER program.[26] For the DGII calculation, bound smoothing was accomplished by using triangle inequalities, and randomized metrization was done to compute a matrix of trial angles among the bond vectors that lie within these limits, and then the matrix was majorized by applying the Guttman transform iteratively. The resulting coordinates were optimized using simulated annealing for 10,000 steps to minimize an error function due to all violations. The correct mirror images were selected based upon the final error function value of 1.0.

To find global minimum structures, we performed restrained energy minimizations using the DISCOVER program (version 2.9.7) for the structures generated by distance geometry calculations.[26] Conjugate gradient minimizations after 1,000 steps of steepest descent minimizations were done to converge into final energy gradients of 0.001 kcal/mol using the same restraints as used in distance geometry calculations. Without explicit solvent molecules, the solvent medium effects of dielectric screening can be effectively mimicked by increasing the dielectric constant. As we reported previously, increased dielectric constant in the potential energy function suppresses overemphasized electrostatic energy terms.[18] All of the glycosidic torsion angles and the structural features were found to be almost idential for dielectric constants from 10.0 to 45.0; thus the results with a dielectric constant of 10 are discussed in this paper.

Results and Discussion

Table 1 summarizes the assignment of ^1H resonances, the coupling constants, and the temperature coefficients of the amido and hydroxyl protons in G_{A1}. As shown in Figure 1a and Figure 1b G_{M1} has sialic acid at the position of IIC3 (third carbon atom in ring II), while G_{A1} does not have any sialic acid. If we compare the chemical shifts of IIH3, IIIH1, and IIIH2 of G_{A1} to the chemical shifts of the same protons reported for G_{M1},[15] there are large downfield shifts for those protons in G_{A1}. There are electrostatic interactions and through-space interactions between the sialic acid, ring II, and ring III in G_{M1}, while in G_{A1} those perturbations to the local magnetic fields do not exist. These differences may give rise to the structural differences between G_{M1} and G_{A1}.

A reduction in temperature susceptibility (ppb/deg) has been commonly accepted as an indicator of reduced interaction with solvent, due to the intramolecular hydrogen bonds. Small temperature coefficients were observed for both the IOH3 proton and the IVOH2 proton. As shown in Figure 2a the very small $^3J_{IH3,IOH3}$, $^3J_{IVH2,IVOH2}$ coupling constants indicate that these hydroxyl protons are involved in strong hydrogen bonds. A very small $^3J_{CH,OH}$ coupling con-

Tertiary Structure of Ganglioside G_A1

Bull. Korean Chem. Soc. **1998**, Vol. 19, No. 5 571

Table 1. Chemical shifts (ppm) referenced to TMS, coupling constants, J(Hz) and temperature coefficients[b] $\kappa(-10^{-3}$ ppm/deg) of G_{A1} in DMSO-d_6

Residue		1	2	3	4	5	6(a,b)	NH	CH₂	CH₃
D-Glc (I)	H	4.157	3.037	3.323	3.285	3.285	3.610 3.742			
	OH		5.086	4.586			4.537			
	J		3.4	<2			5.9			
	κ		8.77	4.35			7.76			
D-Gal (II)	H	4.209	3.233	3.436	3.789	3.489	3.419 3.626			
	OH		5.175	4.737			4.372			
	J		4.6	5.4			4.6			
	κ		9.99	9.37			7.96			
D-GalNAc (III)	H	4.580	3.769	3.653	3.789	3.347	3.503 3.521			1.828
	OH				4.358		4.575	7.463		
	J				4.3		11.6	5.57		
	κ				11.78		7.66	6.15		
D-Gal (IV)	H	4.217	3.324	3.248	3.615	3.317	3.484 3.519			
	OH		3.937	4.687	4.292		4.481			
	J		2.0	5.6	4.5		5.5			
	κ		5.55	11.73	9.05		7.37			
Cer (R)	H	3.424[c]	3.769	3.882	3.355	5.533	1.933		1.234	0.852
	OH	3.975[a]		4.825	1.270[e]	2.021[f]	1.448[g]	7.449		
	J			5.6				8.35		
	κ			8.53				8.40		

[a] Digital resolution is 0.1 Hz/point. [b] Calculated slope from the linear least square analysis of eight data points from 298 K to 333 K. [c] H1a. [d] H1b. [e] Ceramide H7. [f] Ceramide H8. [g] Ceramide H9.
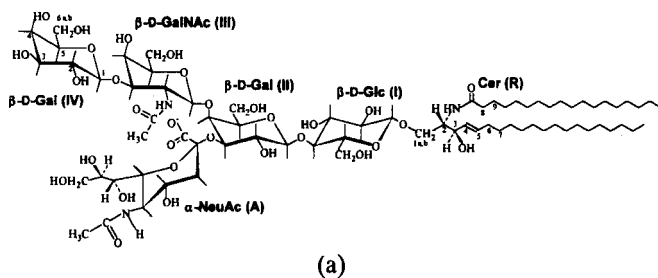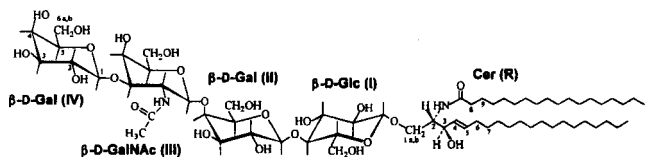
Figure 1. Primary structure of (a) G_{M1} and (b) G_{A1} with symbolism and numbering.

stant or a very big $^3J_{H,OH}$ coupling constant should result from the rigid H-C-O-H configuration by a stable intramolecular hydrogen bond.[12,21] Also, freely rotating hydroxyl groups should show a $^3J_{CH,OH}$ coupling constant with a medium size. It has been reported that IOH3 in G_{M1} has a vanishingly small $^3J_{IH3,IOH3}$ coupling constant, and it may form a stable hydrogen bond with IIO5 in G_{M1}.[12] It has been also reported that G_{M1} may form an intramolecular hy-
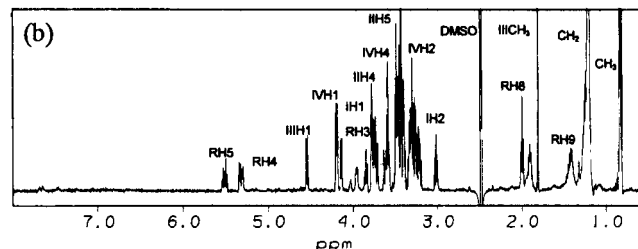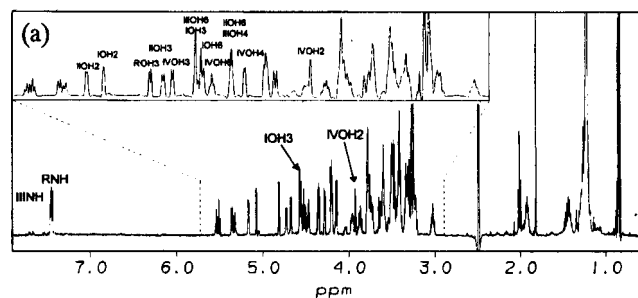
Figure 2. 500-MHz ^{1}H spectrum of 7 mM G_{A1} a) in 100% DMSO-d_6 showing all of the protons including NH and OH exchangeable protons. Some of the important OH protons are labelled. b) in 98:2 DMSO-d_6-D_2O. All of the exchangeable protons are disappeared.

drogen bond between the amido proton in β-D-GalNAc and the carboxyl group in sialic acid that are energetically stabilized.[12] In G_{M1}, the amido proton in β-D-GalNAc has a

Table 2. Interresidual NOE distance restraints of G_{A1} observed in the NOESY spectra with a mixing time of 150 msec, at 303 K

Proton pair	Distance bound (Å)	
	lower	upper
IVH1 / IIIH3	1.8	2.5
IVH1 / IIIH4	1.8	3.1
IVH1 / IIIAc*	1.8	4.8
IVH1 / IIINH	1.8	4.0
IVOH2 / IIIAc*	1.8	5.2
IIIH1 / IIH4	1.8	2.5
IIIAc* / IIH2	1.8	4.5
IIIAc* / IIOH2	1.8	6.1
IIINH / IIH2	1.8	3.7
IIINH / IIOH3	1.8	4.4
IIH1 / IH4	1.8	2.5
IIH1 / IH6a	1.8	3.2
IIH1 / IH6b	1.8	3.3
IIOH2 / IH6a	1.8	4.0
IIOH2 / IH6b	1.8	3.6
IIH1 / IOH3	1.8	3.7
IIH6 / IOH3	1.8	3.7
IIINH / IIIH1	1.8	3.6
IIINH / IIIH2	1.8	3.2
IIINH / IIIH3	1.8	3.4
IIINH / IIIAc*	1.8	3.4

*Pseudo-corrected acetyl group in ring III is denoted by asterisk.

small temperature coefficient of 2.88 ppb/deg and a very big coupling constant (9 Hz).[12] This indicates that the amido proton in the β-D-GalNAc ring in G_{M1} has a fixed orientation by the intramolecular hydrogen bond. Even though in many papers it is mentioned that IOH3 and IVOH2 may be involved in intramolecular hydrogen bond in G_{M1}, the exact positions and strengths of these hydrogen bonds in G_{M1} have not been studied in detail. In G_{A1} the amido proton in β-D-GalNAc has a large temperature coefficient as shown in Table 1 which suggests that this amido proton in G_{A1} does not form a strong intramolecular hydrogen bond. However, the exchange rate of this amido proton is much slower than that of the amido proton in ceramide. This amido proton was shown to remain over one day after exchange with deuterium oxide. Therefore, it is necessary to investigate the intramolecular hydrogen bonds that exist in G_{A1}.

Table 2 shows the interresidual distance restraints calculated from the NOEs observed in NOESY and ROESY spectra with a mixing time of 150 ms at 303 K. In order to avoid spin diffusion problems, the data set with a mixing time of 150 ms among the data sets acquired with the mixing times of 150, 200, and 250 ms was used for the integration. As shown in Figure 2a and Figure 2b, unexchanged hydroxyl protons are fairly well resolved compared to the C-linked protons except the anomeric protons. Unexchanged hydroxyl protons and amido protons in gangliosides protrude farther from the carbon backbone than the C-linked protons and provide NOE contacts with other protons, which can provide additional distance constraints in structural determination. However, it is necessary to discriminate the exchange peaks from the pure NOE peaks betweeen the exchangeable protons in the NOESY spectra.

Figure 3. 500-MHz NOESY spectrum of 7 mM G_{A1} in DMSO-d_6 in the region of the ring protons and the hydroxyl protons a) at 298 K, b) at 303 K, and c) at 313 K. A mixing time of 150 ms was used for these NOESY experiments.

Therefore, we analyzed the NOEs at three different temperatures: 298 K, 303 K, and 313 K. Figures 3a, 3b, and 3c show the NOESY spectrum of G_{A1} at these three temperatures. At 313 K as shown in Figure 3c, 30 contacts between the exchangeable protons are observed in the region between 4 ppm and 5 ppm. At 303 K as shown in Figure 3b, there are about 25 contacts between the exchangeable protons in the region between 4 ppm and 5 ppm. Most of those peaks disappear in the NOESY spectrum at 298 K. At 298 K contacts between the exchangeable protons such as IVOH3/IOH2, IVOH6/IIOH3, IIOH2/IOH3, IOH2/ROH3, and IIINH/IIOH3 remain in the NOESY spectra. At high temperature the exchange rate between the hydroxyl protons becomes faster, and the cross peaks from the exchange phenomena are more prevalent. All of these peaks except IIINH/IIOH3 are observed as exchange peaks in the ROESY spectra. The cross peaks from the exchange phenomena were not included in the NOE integration, and only the contacts listed in Table 2 are included in this calculation. The amido proton in the acetamido group of ring III shows many interresidual NOE contacts with the protons in the sequential residues such as IIOH3, IIH2, and IVH1. These NOE contacts prove that the acetamido group in ring III appears to be closely surrounded by ring II and ring IV and may establish hydrogen bonds between the electronegative atoms in the acetamido group and the IVOH2 proton which has a small coupling constant and a small temperature coefficient. G_{A1} also may have a stable intramolecular hydrogen bond between IOH3 and IIO5, and this is supported by the data including coupling constants and temperature coefficients listed in Table 1 and the NOEs such as IIH1/IOH3 and IIH6/IOH3.

In order to determine the structure of G_{A1} which satisfies all of the experimental data, we need to establish a pool of energetically allowed conformers. In this study we utilized distance geometry calculations. Like in studies on the other gangliosides, the ceramide part of the molecule was excluded in this calculation because there are only few NOEs between the ceramide and sugar rings and also because ceramide is expected to be very mobile. From distance geometry calculations, 30 structures were generated, and root-mean-square deviations (RMSDs) of heavy atoms in all of 30 structures were within 0.5 Å from the average structure. Then, a restrained energy minimization was performed.

In Table 3, the structural features, energies, and the RMSD from the NOE restraints of 10 low-energy structures of GA1 are listed. None of these structures have RMSDs over 0.02 Å from the distance bounds, and these differences between the experimental data and the structures are lower than the experimental error on the NMR distances. Variation of the total energies are not large, ranging from 26.4 to 28.0 kcal/mol. All of these structures have very similar glycosidic torsion angles for the II-I and III-II linkages (within ± 10° variation), while ± 30° variation is observed only for the glycosidic linkage of ring IV and ring III. This is clearly shown in Figure 3, which is the superimposed view of the 30 structures. These 30 structures can be divided into two groups based on the glycosidic torsion angles of the IV-III linkage and the orientation of acetamido group in ring III. The lowest energy structure, G1 in the first group in Table 3, has a set of torsion angles: $\varphi, \psi_{II-I}=$

Table 3. RMSD from distance constraints (Å), total energy (kcal/mol), glycosidic torsion angles φ, ψ, and torsion angles for N-acetyl group, θ_1 and θ_2 in ring III (in degree) for 10 low energy structures of G_{A1} generated by distance geometry calculation and restrained energy minimization

Structure	RMSD	E_{mol}	φ,ψ_{II-I}	φ,ψ_{III-II}	φ,ψ_{IV-III}	$\theta_1,\theta_2{}^a$
G1	0.01	26.4	48, -2	44, 20	39, -30	35, -8
	0.01	27.5	45, -4	45, 21	40, -31	35, -9
	0.02	27.5	49, -1	36, 23	40, -31	35, -8
	0.01	27.7	46, -1	36, 22	37, -29	35, -8
	0.01	27.8	50, -3	45, 22	37, -29	34, -8
	0.01	27.9	48, -1	37, 24	36, -29	34, -8
	0.02	28.0	50, -2	37, 23	40, -30	35, -7
	0.02	28.0	44, -1	36, 18	36, -28	32, -7
G2	0.01	26.4	48, -2	45, 16	10, -12	-175, 0
	0.01	27.9	45, -3	38, 12	14, -14	-175, -1

$^a\theta_1$: H2-C2-N-C, θ_1: C2-N-C-O.
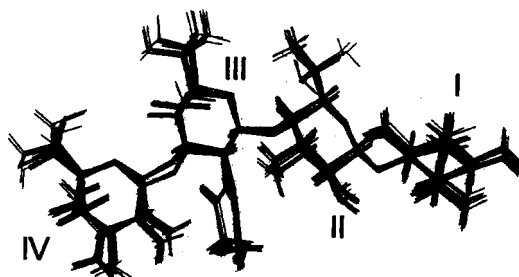
Figure 4. Superposition of 30 structures of G_{A1} generated by DGII calculations.

$48°$, $-2°$; $\varphi,\psi_{III-II}= 44°$, $20°$; $\varphi,\psi_{IV-III}= 39°$, $-30°$; θ_1, $\theta_2=35°$, $-8°$. The lowest energy structure, G2 in the other group has a set of torsion angles; $\varphi,\psi_{II-I}= 48°$, $-2°$; φ, $\psi_{III-II}= 45°$, $16°$; $\varphi,\psi_{IV-III}= 10°$, $-12°$; θ_1, $\theta_2=-175°$, $0°$. G1 has IOH3-IIO5 and IVOH2-IIICO distances of 2.2 Å and 3.7 Å, respectively. G2 has IOH3-IIO5 and IVO2-IIINH distances of 2.2 Å and 2.9 Å, respectively. There are big differences in the orientation of the acetamido group in β-D-GalNAc residue in two groups. Those two low energy structures are shown in Figure 5. As shown in this figure, possible hydrogen bonds are depicted by dotted lines. There is a strong hydrogen bond between IOH3 and IIO5 with a distance around 2.2 Å in every structures. Orientation of acetamido group in G1 allows carbonyl oxygen to be close to the IVOH2, while the orientation of the acetamido group in G2 allows the amido nitrogen to be close to the IVOH2. In the case of G1 group, some of the structures have hydrogen bond between IVOH2 and carbonyl oxygen in acetamido group with a distance of 2.2 Å, but the average distance is 3.4 Å. In the case of G2 group, some of the structures have hydrogen bond between IVOH2 and IIIN with a distance of 2.5 Å, but average distance is 3.0 Å. Therefore, there may be a weak hydrogen bond between the IVOH2 and the acetamido group of ring III. This may be the reason why $^3J_{IH3,IOH3}$ and $^3J_{IVH2,IVOH2}$ are small. Molecular dynamics simulations on G_{A1} in DMSO box should be done to investigate these hydrogen bonds existed in G_{A1} in the near future. All of the structure has low RMS deviation between the structures and low violation from the experimental data,

G1

G2
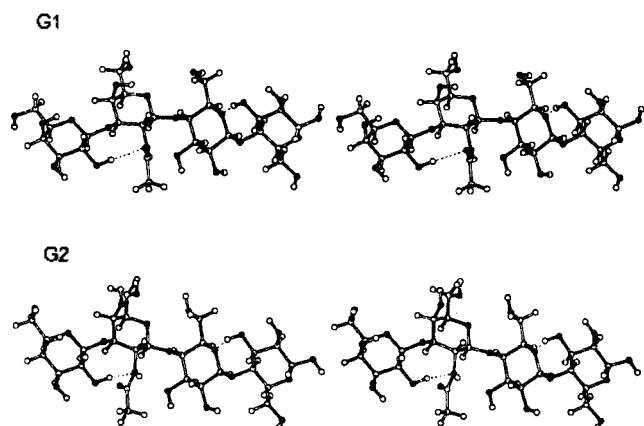
Figure 5. Stereoview of the low-energy structures of G_{A1} showing the possible interresidual hydrogen bonds by dotted lines. Oxygen atom and nitrogen atom are marked with filled circles.

which implicates that these structures are very similar to each other except that there are local structural variations in the linkages of ring III and ring IV.

Table 4 lists the glycosidic torsion angles for the low-energy structure of gangliosides, G_{M1}, G_{M1b}, and G_{A1} as determined by NMR spectroscopy or by theoretical calculations. Structural data reported by Scarsdale *et al.*[15] are obtained from the restrained molecular mechanics calculations. The structure of G_{M1} reported by Acquotti *et al.*[12] is calculated by the distance mapping method. The structure of G_{A1} has been also calculated theoretically without experimental data,[29] and it is similar to that of G1 reported in this study. Even though all of these structures are calculated by the different methods, we compared the structural data of G_{A1} to the other data in order to understand the relationships between the structures and the functions of different gangliosides. All of the ganglioside have very similar torsion angles in β-D-Gal-(1→4)-β-D-Glc linkage which correspond to the lowest energy structure of lactose.[18] Surprisingly, the structure of G_{M1}[15] is very similar to the structure of G1 even though there is no sialic acid in G_{A1}. Since G_{M1b} has sialic acid attached to the ring IV instead of ring II, the torsion angles of the III-II linkage and IV-III linkage in G_{M1} are different from those in G_{M1b}. The ψ torsion angle in the III-II linkage in G_{M1b} is about 70° different from that in G1 and G2. Unfortunately, data related to the hydrogen bonds in these structures are not available; thus only the overall foldings of these structures can be compared. As reported

before, the polar sialic acid unit in G_{M1} generates the intramolecular hydrogen bondings with the acetamido group in ring III. Because the structures of G_{M1} and G_{A1} are very similar, these additional hydrogen bonds do not seem to have a profound influence on the overall structural folding in G_{M1}.

Conclusions

As shown in this study, distance geometry calculations are demonstrated to be good ways to generate the structures of gangliosides using NMR experimental data. There are two low-energy structures for G_{A1}, G1 and G2. G1 is different from G2 only in the IV-III glycosidic linkage and the orientation of the acetamido group in ring III. There is a stable intramolecular hydrogen bond between the third hydroxyl group in ring I and the ring oxygen atom in ring II. They also show that there may be a weak hydrogen bond between the second hydroxyl group in ring IV and the acetamido group in ring III. Since the acetamido group in the β-D-GalNAc unit is surrounded by ring II and ring IV in a compact manner, this amido proton cannot interact with the solvent easily. This may be the reason for its slow exchange. Also, the temperature coefficient of this amido proton is much smaller than that of amido proton in ceramide.

G_{M1}, which has a polar sialic acid, has intramolecular hydrogen bonds between the amido proton in β-D-GalNAc and the carboxylic oxygen in the sialic acid and is energetically stabilized. These electrostatic interactions and through-space interactions between the sialic acid, which is linked to IIC3 and core residues in G_{M1}, cause the chemical shift perturbations in G_{M1}. There are more chemical shift dispersions in G_{M1} than in G_{A1}. However, this study shows that tertiary foldings of G_{A1} are very similar to those in G_{M1}. We suggest that the differences in the biological specificities between G_{M1} and G_{A1} are caused not by their tertiary foldings, but mainly by electrostatic properties due to the presence or absence of sialic acid. Since it is evident that G_{A1} is more hydrophobic than G_{M1}, a surface ligand with a hydrophobic binding site can recognize the G_{A1} better than G_{M1}. Therefore, the epitopes of the pathogens which bind to the G_{A1} receptor should have hydrophobic properties. The results on the conformation of G_{A1} obtained from this work is expected to be useful in understanding of the recognition of gangliosides at the membrane surface.

Table 4. Comparison of the glycosidic angles of G1 and G2 to the angles reported previously for G_{M1}, G_{M1b}, and G_{A1}

		G_{M1}[15]	G_{M1}[12]	G_{M1b}[15]	G_{A1}[29]	G_{A1}(G1)*	G_{A1}(G2)*
II-I	φ	48	50	49	52	48	48
	ψ	−23	0	−21	−4	−2	−2
III-II	φ	26	40	−9	50	44	45
	ψ	45	25	−46	1	20	16
IV-III	φ	46	34	16	51	39	10
	ψ	−47	30	−29	0	−30	−12

*this paper.

References

1. Dwek, R. A.; Quiocho, F. *Curr. Opin. in Struct. Biol.* **1991**, *1*, 709.

2. Yoon, H.; Park, H.; Jhon, G. *Biochemistry Int.* **1992**, *28*, 393.

3. Ledeen, R. W.; Wu, G. *Trends Glycosci. Glycotechnol.* **1992**, *4*, 174.

4. Fishman, P. H., In *New Trends in Ganglioside Research*,

Spectroscopic Properties of cis-[Cr(trien)Cl₂]Cl

Bull. Korean Chem. Soc. **1998**, Vol. 19, No. 5   575

Ledeen, R. W.; Hogan, E. L.; Tettamanti, G.; Yates, A. J.; Yu, R. K., Eds.; Liviana Press: Padova, Italy, 1988.

5. Sachinidis, A.; Kraus, R.; Seul, C.; Meyer, Z.; Brickwedde, M. K.; Schulte, K.; Ko, Y.; Hoppe, J.; Veter, H. *Eur. J. Cell Biol.* **1996**, *71*, 70.

6. Silva, R. H.; Felicio, L. F.; Nasello, A. G.; Viral, M. A. B. F.; Frussa, F. R. *J. Aging.* **1996**, *17*, 583.

7. Hakomori, S. I. *J. Biol. Chem.* **1990**, *265*, 18713.

8. Brennan, M. J.; Hannah, J. H.; Leininger, E. *J. Biol. Chem.* **1991**, *266*, 18827.

9. Yu, L.; Lee, K. K.; Hodges, R. S.; Paranchych, W.; Irvin, R. *Infect. Immun.* **1994**, *62*, 5213.

10. Imundo, L.; Barasch, J.; Prince, A.; Al, A. Q. *Proc. Natl. Acad. Sci. USA* **1995**, *92*, 3019.

11. Yu, L.; Lee, K. K.; Sheth, B.; Lane-Bell, P.; Seivastava, G.; Hindsgaul, O.; Paranchych, W.; Hodges, R. S.; Irvin, R. T. *Infect. Immun.* **1994**, *62*, 2843.

12. Acquotti, D.; Poppe, L.; Dabrowski, J.; Lieth, C.; Sonnino, S.; Tettamanti, G. *J. Am. Chem. Soc.* **1990**, *112*, 7772.

13. Acquotti, D.; Fronza, G.; Ragg, E.; Sonnino, S. *Chem. Phys. Lipids* **1991**, *59*, 107.

14. Sabesan, S.; Duus, J. O.; Fukunaga, T.; Bock, K.; Ludvigsen, S. *J. Am. Chem. Soc.* **1991**, *113*, 3236.

15. Scarsdale, J. N.; Prestegard, J. H.; Yu, R. *Biochemistry* **1990**, *29*, 9843.

16. Siebert, H.; Reuter, G.; Schauer, R.; Lieth, C.; Dabrowski, J. *Biochemistry* **1992**, *31*, 6962.

17. Lee, K.; Jhon, G.; Rhyu, G.; Bang, E.; Choi, B.; Kim, Y. *Bull. Korean Chem. Soc.* **1995**, *16*, 864.

18. Oh, J.; Kim, Y.; Won, Y. *Bull. Korean Chem. Soc.* **1995**, *16*, 1153.

19. Shim, G.; Lee, S.; Kim, Y. *Bull. Korean Chem. Soc.* **1997**, *18*, 415.

20. Bevilacqua, V. L.; Kim, Y.; Prestegard, J. H. *Biochemistry* **1992**, *31*, 9339.

21. Lee, K.; Kim, Y. *Bull. Korean Chem. Soc.* **1996**, *17*, 118.

22. Bax, A.; Davis, D. G. *J. Magn. Reson.* **1985**, *65*, 355.

23. Macura, S.; Ernst, R. R. *Mol. Phys.* **1980**, *41*, 95.

24. Derome, A.; Willamson, M. *J. Magn. Reson.* **1990**, *88*, 177.

25. Bax, A. Davis, D. G. *J. Magn. Reson.* **1985**, *63*, 207.

26. Molecular Simulations Inc., San Diego, CA, USA.

27. Havel, T. F. *Prog. Biophys. Mol. Biol.* **1991**, *56*, 43.

28. Homans, S. W. *Biochemistry* **1990**, *29*, 9110.

29. Park, H.; Jhon, G.; Han, S.; Kang, Y. *Biopolymers* **1997**, *42*, 19.

Luminescence, Excitation and Far-Infrared Spectroscopy of cis-α-Dichlorotriethyleneteraminechromium(III) Chloride

Jong-Ha Choi

Department of Chemistry, Andong National University, Andong 760-749, Korea
Received February 19, 1998

The 77 K luminescence and excitation spectra, and 298 K infrared and absorption spectra of cis-α-[Cr(trien)Cl₂] Cl·H₂O (trien=triethylenetetramine) have been measured. Ligand field electronic transitions due to spin-allowed and spin-forbidden are assigned. The zero-phonon line in the excitation spectrum splits into two components by 198 cm⁻¹, and the large ^2E_g splitting can be reproduced by the modern ligand field theory. It is confirmed that nitrogen atoms of the trien ligand have a strong σ-donor character, but chloride ligand has weak σ- and π-donor properties toward chromium(III) ion.

Introduction

The synthesis, kinetics of aquation, absorption and infrared spectral data and ligand field photolysis of the dichlorochromium(III) complex containing linear quadridentate triethylenetetramine (trien=2,2,2-tet) ligand have been studied.[1-3] However, the vibrational and electronic energy levels based on the luminescence and excitation spectroscopy of title complex have not been known yet. The sharp-line electronic spectroscopic techniques offer promise in obtaining geometric informations, especially in noncrystalline environments, and in determining metal-ligand bonding properties.[4,5]

In this study the luminescence, excitation and infrared spectra of cis-α-[Cr(trien)Cl₂]Cl H₂O were measured. The vibrational intervals of the electronic state were determined from the far-infrared and luminescence spectra. The pure electronic origins were assigned by analyzing the absorption and excitation spectra. Using observed electronic transitions, a ligand field analysis has been performed to determine the detailed bonding properties for the coordinated chloride and nitrogen atoms toward chromium(III) ion.

Experimental Section

Anhydrous chromium(III) chloride and ligand trien (Aldrich, technical grade) were used without further purification. All other commercially available chemicals were reagent grade. The cis-α-[Cr(trien)Cl₂]Cl·H₂O was prepared according to the published method.[1] The measured visible